AIMS Mathematics, 11(1): 2430–2457.
DOI: 10.3934/math.2026099
Received: 18 December 2025
Revised: 06 January 2026
Accepted: 14 January 2026
Published: 26 January 2026

https://www.aimspress.com/journal/Math

Research article

High-reliability cooperative guidance law design considering link failure and input saturation

Zewei Liu[1] **and Zhanpeng Gao**[2,*]

[1] School of Mechanical Engineering, Sichuan University, Chengdu 610065, China

[2] Department of Electrical and Computer Engineering, National University of Singapore, Singapore 117583, Singapore

* **Correspondence:** Email: gaozhanpeng@njust.edu.cn.

Abstract: In the context of electronic countermeasures, addressing the issues of acceleration saturation and unreliable communication links during multi-vehicle cooperative guidance, an adaptive high-reliability cooperative guidance law with relative impact velocity and impact angle constraints is proposed. First, an online target acceleration estimator based on a nonlinear disturbance observer (NDO) is constructed to improve robustness against maneuvering targets and uncertain disturbances. On this basis, a state-dependent adaptive term is introduced into the traditional double power reaching law to effectively mitigate the impact of acceleration saturation on guidance stability. Second, addressing the scenario of communication link interruptions, a fixed-time open-loop cooperative strike fault-tolerant backup guidance law is designed, along with a smooth switching strategy for control variables, thereby enhancing the reliability of the overall guidance process. Simulation results under various conditions, including ideal scenarios and communication interruptions, demonstrate that the proposed cooperative guidance law can achieve cooperative attacks on maneuvering targets with the desired relative impact kinetic energy and impact angles. The adaptive term effectively attenuates overload saturation and enhances guidance stability, while the system can rapidly switch to the fault-tolerant scheme to ensure mission completion even under communication interruption. Monte Carlo simulations further verify the adaptability and robustness of the proposed method under parameter perturbations and uncertain initial conditions.

Keywords: terminal angle constraint; impact speed constraint; fault-tolerant control; guidance law
Mathematics Subject Classification: 93D05, 93D40

1. Introduction

In modern warfare, cooperative guidance technology is particularly critical for countering high-speed moving targets and striking key enemy bases [1, 2]. During the cooperative engagement of multiple flight vehicles, each vehicle can acquire different new information and exchange it with others, and such information interaction enhances the scalability of mission execution. Even if individual vehicles fail, the system can still ensure successful completion of the combat mission [3].

Cooperative control of flight vehicles refers to a tactic that improves strike effectiveness by coordinating the behavior of multiple vehicles. At present, two main cooperative schemes are adopted, namely distance-cooperative guidance [4, 5] and impact-time-cooperative guidance [6, 7].

Most existing studies achieve cooperative strikes by controlling the flight vehicles such that their remaining flight times converge to a common value [8]. Chen et al. [9] designed a robust cooperative guidance law that ensures multiple vehicles accomplish the mission at the same time with different impact angles. Although the impact angles can rapidly converge to the desired values, the corresponding control inputs exhibit numerous abrupt changes, making this method impractical for engineering applications. Xiong et al. [10] proposed an heterogeneous multi-vehicle cooperative guidance strategy (HKGG) cooperative guidance strategy that does not require a predesigned communication topology; however, the simulations in that work were conducted under an interference-free communication environment, so its adaptability and robustness are difficult to guarantee.

For engagement against moving targets, Li et al. [11] designed a cooperative guidance law with impact-time constraints. The proposed guidance system can achieve finite-time stability and intercept maneuvering targets; nevertheless, in the simulations, the acceleration is limited to 25×g while full overload still occurs, implying huge energy consumption and rendering its practical implementation difficult. Wang et al. [12] proposed an robust cooperative guidance law (RTCGL) cooperative guidance law and, combined with a filtering algorithm, developed a robust cooperative guidance method for maneuvering targets. Although this scheme is simple to implement, its control inputs fluctuate significantly, which may lead to instability in the guidance process. Wang et al. [13] further proposed a prescribed-time cooperative guidance law (PTCGL) cooperative guidance law and introduced an auxiliary coefficient to handle input saturation; however, the simulation results still exhibit oscillations and saturation in the control input. He et al. [14] designed a leader–follower cooperative guidance law with fixed-time convergence, yet the control inputs still show substantial oscillations. Zhan et al. [15] used a time-varying sliding mode to design a cooperative guidance law; although it is claimed that excessively large initial accelerations can be avoided, acceleration saturation still occurs, and the large variation in acceleration during the guidance process leads to increased energy consumption. Dong et al. [16] designed a guidance law with fixed-time convergence, but the control inputs in their simulation results exhibit frequent acceleration jumps and saturation, indicating that the proposed guidance law does not meet practical engineering requirements. Guo et al. [17] adopted a novel remaining flight time estimation method and used t_{go} as the coordination variable to design a cooperative guidance law; communication delays and packet losses were considered in the simulations. However, under electronic countermeasures, communication mechanisms may completely fail, and thus the proposed guidance law is not suitable for highly complex combat environments.

Instead, a number of studies use the remaining flight distance as the coordination variable to achieve

cooperative guidance. Li et al. [18] adopted a leader–follower guidance strategy based on remaining-distance coordination, and the simulation results show that consensus can be achieved at the prescribed time under different initial conditions. Zhang et al. [19] designed a cooperative guidance law whose simulation results exhibit chattering in the terminal phase, which poses a significant challenge for actuators in practical applications. In the guidance law proposed by Wang et al. [20], the leader vehicle adopts proportional navigation, whereas the follower vehicles employ a PTCGL algorithm to guarantee convergence of the line-of-sight (LOS) angles at a specified time; however, all simulations were conducted in an ideal communication environment. Liu et al. [21] combined reasoning and drag models and designed a guidance law using a sliding-mode algorithm, enabling multiple low-speed vehicles to intercept a hypersonic target. Chen et al. [22] proposed an event-triggered cooperative guidance law, claiming that reducing the frequency of cooperative communication can lower energy consumption. Nevertheless, for hypersonic vehicles, communication gaps lead to larger position deviations, and the energy required to adjust the attitude and position can far exceed the energy consumption of communication. Moreover, the acceleration exhibits large jumps, and the introduction of event-triggering makes it difficult for actuators to accomplish the task. Under electronic countermeasures, the communication function may be severely disturbed, affecting task execution. The abovementioned cooperative guidance laws, which are all established under ideal conditions, cannot adapt to complex combat environments.

Strategies involving communication topology switching have been adopted in the literature [23, 24] to prevent failures caused by interference and deception attacks [25]. In the context of cooperative guidance, Chen et al. [26] incorporated this strategy to formulate a piecewise guidance law for stationary targets, integrating a terminal sliding mode with proportional navigation. Although Yu et al. [27] suggested that topology switching could handle communication faults, their method suffers from significant drawbacks: The resulting acceleration exhibits saturation exceeding 20 seconds and experiences frequent sudden jumps, placing excessive stress on the actuators. In a subsequent study, Yu et al. [28] developed a fixed-time convergent guidance law tested against communication failures. However, their fault model assumes that agents can receive data but cannot transmit them, which lacks physical validity and fails to represent actual complete outages. Consequently, under intense electronic countermeasures, relying solely on topology switching is inadequate, as genuine communication interruptions often lead to the failure of cooperative strikes.

This paper focuses on the cooperative terminal guidance problem of multiple flight vehicles under modern electronic countermeasure conditions. To address key engineering challenges, including the dual constraints on the relative impact velocity and attack angle, the potential stability risks caused by acceleration saturation, and cooperative failure caused by interruptions of the communication link, a highly reliable cooperative guidance framework is constructed that combines online disturbance observation, adaptive shaping of the reaching law, and a fault-tolerant backup guidance scheme. On this basis, a systematic study is carried out from three perspectives, namely enhancement of the terminal performance constraints, improving stability during the guidance process, and ensuring mission reliability in complex combat environments.

The contributions of this paper are as follows.

(1) A cooperative guidance framework for multiple flight vehicles is proposed that explicitly constrains both the relative impact velocity and the impact angle. A disturbance observer is introduced into the guidance law to perform online estimation of target acceleration and external

disturbances, thereby enabling cooperative engagement of maneuvering targets in uncertain environments.

(2) To address the acceleration saturation that easily arises during the guidance process, a state-dependent adaptive term is embedded into the conventional double power reaching law, and an adaptive high-reliability cooperative guidance law is constructed. This law effectively suppresses overload saturation and alleviates control chattering, while improving the smoothness of control commands and the stability of the closed loop system without sacrificing guidance accuracy.

(3) For communication link interruptions under modern electronic countermeasure conditions, a fault-tolerant backup guidance law for fixed time open loop cooperative engagement is designed, together with a smooth switching mechanism between the primary and backup guidance laws. This design allows multiple flight vehicles to maintain cooperative terminal performance even in the presence of communication interruptions. Multi scenario and Monte Carlo simulations verify the reliability and adaptability of the proposed method.

This paper is structured as follows. Following the introduction, the problem's formulation and guidance modeling are described in Section 2. Section 3 focuses on the construction of the observer. In Section 4, the proposed adaptive high-reliability cooperative guidance strategy is derived. The effectiveness of the method is illustrated through simulation results in Section 5, followed by concluding remarks in Section 6.

2. Problem description

2.1. Flight vehicles' communication topology

This paper investigates the scenario where multiple flight vehicles cooperate to intercept maneuvering hostile targets simultaneously. To describe the information exchange structure within the cooperative cluster, an undirected graph $G = (\varepsilon, \xi, \tau)$ is used to model the communication topology. Specifically, ε denotes the set of nodes, with ε_i corresponding to the i-th flight vehicle. The set of edges ξ depicts the communication links among the vehicles, whereas τ represents the weighted adjacency matrix. According to [29, 30], the elements of τ are defined as

$$a_{ij} = \begin{cases} a_{ij} > 0, & \varepsilon_i, \varepsilon_j \in \varepsilon, \\ a_{ij} = 0, & \varepsilon_i, \varepsilon_j \notin \varepsilon. \end{cases} \tag{2.1}$$

The Laplacian matrix corresponding to the graph G is denoted as $\mathcal{L} = [l_{ij}] \in \mathcal{R}^{n\times n}$, wherein the specific entries l_{ij} are given by:

$$l_{ij} = \begin{cases} \sum_{t=1,t\neq i}^{n} a_{it}, & t = i, \\ -a_{ij}, & t \neq i. \end{cases} \tag{2.2}$$

2.2. Related lemma

Definition 2.1. [8] For a second-order system, if there is a time instant t^* such that the system states can evolve from arbitrary initial values to the desired target state for all $t \geq t^*$, then the system variables are said to achieve consensus within finite time. The dynamics of the second-order system

are described by:

$$\begin{cases} \dot{x}_{1i} = x_{2i}, \\ \dot{x}_{2i} = u_i. \end{cases} \tag{2.3}$$

Lemma 2.1. [31] Consider a second-order system where the communication network among agents is characterized by an undirected connected topology. Under the influence of the consensus control input u_i, the system is guaranteed to achieve convergence within a finite time horizon.

$$u_i = -\gamma_1 sig\left[\sum_{l=1}^{n} a_{il}\left(x_{1i} - x_{1l}\right)\right]^a - \gamma_2 sig\left[\sum_{l=1}^{n} a_{il}\left(x_{2i} - x_{2l}\right)\right]^{\frac{2a}{1+a}}. \tag{2.4}$$

In the formula, a_{il} is the weight of the undirected graph, and $\gamma_i > 0, i = 1, 2; 0 < a < 1$, where $sig^a(x) = |x|^a sgn(x)$.

Lemma 2.2. [32] Consider the nonlinear system described by

$$\begin{cases} \dot{x}\left(t\right) = f\left(x\left(t\right)\right), \\ x\left(0\right) = x_o, \end{cases} \tag{2.5}$$

where x and f represent the system's state vector and the nonlinear dynamics, respectively. Finite-time stability is achieved if there is a continuously differentiable function V satisfying the inequality $\dot{V}(x(t)) \leq -tV^n(x(t))$. Here, t is a positive constant and the exponent n lies in the range $0 < n < 1$. The convergence time is bounded by

$$T_s < \frac{1}{t\left(1-n\right)} \left|V\left(x_0\right)\right|^{1-n}. \tag{2.6}$$

Lemma 2.3. [33] Given the system $\dot{x} = f(t, x)$ with a positive definite function $V(x)$, suppose that the following inequality holds

$$\dot{V}\left(x\right) \leq -\mu_1 V^{\alpha}\left(x\right) - \mu_2 V^{\beta}\left(x\right) + C, \tag{2.7}$$

where $\mu_1 > 0$, $\mu_2 > 0$, $C > 0$, $\alpha \in (1, +\infty)$, and $\beta \in (0, 1)$. In this case, the system exhibits practically fixed-time stability, and all signals of the closed-loop system will converge to a residual set within the settling time T_s. The residual set can be depicted as

$$\Omega = \left\{ \lim_{t \to T_s} x \,\middle|\, V(x) \leq \min\left\{ \mu_1^{-\frac{1}{\alpha}} \left(\frac{C}{1-\phi}\right)^{\frac{1}{\alpha}}, \mu_2^{-\frac{1}{\beta}} \left(\frac{C}{1-\phi}\right)^{\frac{1}{\beta}} \right\} \right\}, \tag{2.8}$$

where $\phi \in (0, 1)$ is a scalar parameter, and the settling time T_s is bounded by

$$T_s \leq \frac{1}{\mu_1 \phi(\alpha - 1)} + \frac{1}{\mu_2 \phi(1-\beta)}. \tag{2.9}$$

Lemma 2.4. [34] For any $m > 1, n > 1, (m-1)(n-1) = 1, x, y \in R, \varepsilon > 0$, we have

$$xy \leq \frac{\varepsilon^m}{m} |x|^m + \frac{1}{n\varepsilon^n} |y|^n. \tag{2.10}$$

Lemma 2.5. [35] For any $x \in R, \varepsilon \in R^+$, we have

$$0 \leq |x| - \frac{x^2}{\sqrt{x^2 + \varepsilon^2}} < \varepsilon. \tag{2.11}$$

Lemma 2.6. [36] Given a set of non-negative real numbers $x_t \geq 0$ for $t = 1, 2, \ldots, k$, the following relationship holds:

$$\left(\sum_{t=1}^{k} x_t\right)^2 \leq k \sum_{t=1}^{k} x_t^2. \tag{2.12}$$

Lemma 2.7. [37] For the arbitrary real variables $x_k \in R$ and a parameter $t \in [0, 1]$ $(k = 1, 2, \ldots, m)$, the following relation is satisfied:

$$(|x_1| + \ldots + |x_m|)^t \leq |x_1|^t + \ldots + |x_k|^t . \tag{2.13}$$

Lemma 2.8. [38] Given the arbitrary positive real numbers $x, k, \delta \in R^+$, the following inequality is valid:

$$k\delta \geq |x| - x\tanh\left(\frac{x}{\delta}\right). \tag{2.14}$$

2.3. Relative motion model

As shown in Figure 1, a model for the cooperative interception of maneuvering targets by multiple flight vehicles in a two-dimensional plane is established. In this model, M_i and T represent the positions of the flight vehicle and the target, respectively; $\theta_{M/T}$ is the trajectory inclination angle; q_i is the flight vehicle-to-target LOS angle; $a_{M/T}$ is the normal overload of the flight vehicle and target; $V_{M/T}$ represents the velocity of the flight vehicle and target; and R_i represents the relative range between the i-th flight vehicle and the target.

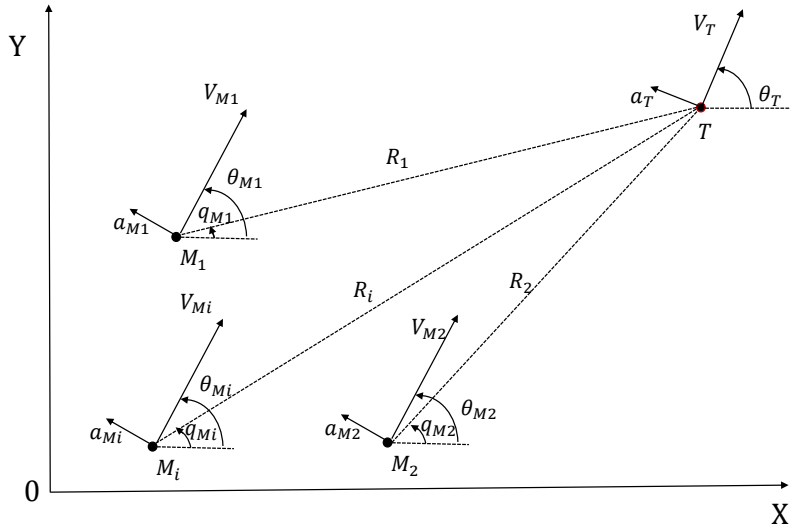

Figure 1. Relative motion relationship between the flight vehicle and the target.

To facilitate the subsequent analysis and controller design, the following assumptions are established.

Assumption 2.1. [39] Both the flight vehicle and the target are modeled as point masses. It is assumed that the relative state variables R, θ_M, and q_M are measurable, and the flight vehicle maintains a speed advantage over the target.

Assumption 2.2. [40] The autopilot is treated as an ideal system, where dynamic lags and response delays are neglected.

Assumption 2.3. [41] The velocity vector of the flight vehicle is assumed to be collinear with its longitudinal body axis, implying that the angle of attack is zero.

Assumption 2.4. [42] The acceleration components of the maneuvering target along all three axes, as well as their time derivatives, are assumed to be bounded.

The following relative motion equation can be derived from Figure 1:

$$\dot{R}_i = V_T cos(\theta_T - q_i) - V_{Mi} cos(\theta_{Mi} - q_i), \tag{2.15}$$

$$\dot{q}_i = \frac{V_T sin(\theta_T - q_i) - V_{Mi} sin(\theta_{Mi} - q_i)}{R_i}, \tag{2.16}$$

$$\dot{\theta}_{Mi} = \frac{a_{Mi}}{V_{Mi}}, \tag{2.17}$$

$$\dot{\theta}_T = \frac{a_T}{V_T}. \tag{2.18}$$

Taking the time derivatives of Eqs (2.15) and (2.16) yields:

$$\begin{cases} \ddot{R}_i = R_i \dot{q}_i^2 - M_{Ri} + T_{Ri}, \\ \ddot{q}_i = -\dfrac{2\dot{R}_i \dot{q}_i}{R_i} - \dfrac{M_{qi}}{R_i} + \dfrac{T_{qi}}{R_i}. \end{cases} \tag{2.19}$$

Here, M_{Ri} and T_{Ri} denote the acceleration components of the flight vehicle and the target projected along the LOS direction. Furthermore, M_{qi} and T_{qi} correspond to the acceleration components perpendicular to the LOS. The specific expressions are defined as follows:

$$\begin{cases} M_{Ri} = a_{Mri} \cos(q_i - \theta_{Mi}) + a_{Mi} sin(q_i - \theta_{Mi}), \\ M_{qi} = -a_{Mri} sin(q_i - \theta_{Mi}) + a_{Mi} cos(q_i - \theta_{Mi}), \\ T_{Ri} = a_{Tr} \cos(q_i - \theta_T) + a_T sin(q_i - \theta_T), \\ T_{qi} = -a_{Tr} sin(q_i - \theta_T) + a_T cos(q_i - \theta_T). \end{cases} \tag{2.20}$$

In the formulation, a_{Mri} and a_{Mi} denote the acceleration components of the flight vehicle tangent and normal to its velocity vector, respectively. Similarly, a_{Tr} and a_T correspond to the tangential and normal acceleration components of the target. Consequently, the center-of-mass kinematic equations governing both the flight vehicle and the target are expressed as:

$$\begin{cases} \dot{X}_{M/T,i} = V_{M/T,i} cos\theta_{M/T,i}, \\ \dot{Y}_{M/T,i} = V_{M/T,i} sin\theta_{M/T,i}. \end{cases} \tag{2.21}$$

2.4. Guidance law model

The state-space of the LOS direction subsystem can be expressed as follows. By synthesizing the relative motion kinematics with the center-of-mass dynamics, the flight vehicle–target system can be decoupled into two orthogonal subsystems: aligned with the LOS and the other normal to it to ensure that the terminal requirements for the impact angle and relative velocity are met while engaging a maneuvering target. Defining the state variables as $x_{1i} = R_i$, $x_{2i} = \dot{R}_i$, $x_{3i} = q_i - q_{exp,i}$, and $x_{4i} = \dot{q}_i$, and substituting them into Eq (2.19), we obtain the following state-space equation.

The state-space representation for the LOS direction subsystem is formulated as:

$$\begin{cases} \dot{x}_{1i} = x_{2i}, \\ \dot{x}_{2i} = x_{1i}x_{4i}^2 - M_{Ri} + T_{Ri}. \end{cases} \tag{2.22}$$

Correspondingly, the state-space equation governing the subsystem normal to the LOS is given by:

$$\begin{cases} \dot{x}_{3i} = x_{4i}, \\ \dot{x}_{4i} = -\dfrac{2x_{2i}x_{4i}}{x_{1i}} - \dfrac{M_{qi}}{x_{1i}} + \dfrac{T_{qi}}{x_{1i}}. \end{cases} \tag{2.23}$$

In this formulation, $q_{\exp,i}$ denotes the desired LOS angle. Assuming the velocity is controllable, an acceleration component M_{Ri} is induced along the LOS axis. Consequently, the control strategy can be decoupled into a dual-channel architecture. In the LOS channel, a guidance law is synthesized to ensure the interception of the maneuvering target with a prescribed relative impact velocity. Simultaneously, in the normal channel, a separate guidance law is formulated to guarantee that the flight vehicle strikes the target at the required terminal impact angle. The specific design objectives are summarized as follows:

$$\begin{cases} \lim\limits_{t\to T_f} x_{1i} \le \varpi, \quad \lim\limits_{t\to T_f} |x_{2i} - V_{exp}| \le \varpi, \\ \lim\limits_{t\to T_f} |x_{3i}| \le \varpi, \quad \lim\limits_{t\to T_f} |x_{4i}| \le \varpi, \end{cases} \tag{2.24}$$

where T_f is the actual flight time of the flight vehicle, ϖ is a tiny positive scalar representing the allowable tracking error bound, and $V_{\exp}$ is the relative velocity between the flight vehicle and the target.

3. Nonlinear disturbance observer

3.1. The observer's design

In practical interception scenarios, the target's maneuvering accelerations (i.e., T_{Ri} and T_{qi}) represent unknown a priori information for the interceptor. Therefore, in this paper, these maneuvering terms, along with other unmodeled system dynamics, are collectively defined as lumped disturbance. To effectively compensate for these unknown perturbations, an observer is employed to perform real-time online estimation of both internal and external disturbances.

In this section, a nonlinear disturbance observer (NDO) is proposed, which incorporates the adaptive law described in Eq (3.3) to approximate the disturbance's upper bound. This strategy successfully alleviates the limitation of needing prior information regarding the amplitude of external mismatched disturbances [43].

The structure of the proposed observer is given by:

$$\hat{d}_i = k_{i1}\pi_i + k_{i2}\frac{\pi_i}{\sqrt{\pi_i^2 + \left(\frac{\varepsilon_i}{k_{i2}}\right)^2}} + k_{i3}\pi_i^3 + \hat{p}_i \tanh\left(\frac{\hat{p}_i\pi_i}{\delta_i}\right), \tag{3.1}$$

where ε_i, k_{i1}, k_{i2}, and k_{i3} are the parameters to be designed; $\hat{p}_i$ is the estimated upper bound of the disturbance signal; and π_i is an auxiliary variable, that is specified as follows:

$$\pi_i = x_i - s_i, \tag{3.2}$$

$$\dot{\hat{p}}_i = |\pi_i| - \frac{\sigma_{i1}}{n_i}\hat{p}_i - \frac{\sigma_{i2}}{n_i^2}\hat{p}_i^3. \tag{3.3}$$

Let $\widetilde{p}_i = p_i - \hat{p}_i$, where s_i is specifically given as

$$\dot{s}_i = k_{i1}\pi_i + k_{i2}\frac{\pi_i}{\sqrt{\pi_i^2 + \left(\frac{\varepsilon_i}{k_{i2}}\right)^2}} + k_{i3}\pi_i^3 + \hat{p}_i \tanh\left(\frac{\hat{p}_i\pi_i}{\delta_i}\right) + f_i + b_i x_{i+1}. \tag{3.4}$$

Here, n_i, σ_{i1}, and σ_{i2} constitute the design parameters. The estimation error of the disturbance signal is defined as $\widetilde{d}_i = d_i - \hat{d}_i$. By synthesizing Eqs (3.2) and (3.4), the dynamics can be derived as $\dot{\pi}_i = d_i - \hat{d}_i = \widetilde{d}_i$. Within this proposed novel disturbance observer framework, the adaptive term $\hat{p}_i \tanh\left(\frac{\hat{p}_i\pi_i}{\delta_i}\right)$ is incorporated to facilitate smooth switching. In contrast to conventional observers, the proposed scheme guarantees finite-time convergence.

Remark 3.1. The selection of the NDO parameters k_{i1} and ε_i is critical for balancing the estimation's accuracy and the system's stability. Specifically, the linear gain k_{i1} determines the fundamental convergence speed of the observer; it is tuned by gradually increasing its value to ensure fast tracking of the target's maneuver, bounded by the threshold where sensor noise amplification becomes detrimental. The parameter ε_i regulates the smoothness of the nonlinear function, acting as a boundary layer's thickness. A smaller ε_i yields higher estimation precision by closely approximating the sign function but risks inducing high-frequency chattering, whereas a larger ε_i ensures smoother control signals at the expense of steady-state accuracy.

3.2. Stability proof

Theorem 3.1. Provided that the observer is constructed according to Eq (3.1) and assuming that the disturbances addressed in this study remain bounded, the proposed disturbance observer guarantees that the estimation errors π_i and $\widetilde{p}_i$ will converge to a residual set near the origin within a finite-time duration T_d, bounded by $T_d \leq \frac{2}{t_1} + \frac{1}{t_2}$.

Proof. Consider the Lyapunov function candidate defined by:

$$V_d = \sum_{i=1}^{n}(\frac{1}{2}\pi_i^2 + \frac{1}{2}\widetilde{p}_i^2). \tag{3.5}$$

Taking the derivative, we get:

$$\begin{aligned}\dot{V}_d &= \sum_{i=1}^{n}(\pi_i\,\dot{\pi}_i + \widetilde{p}_i\dot{\widetilde{p}}_i)\\ &= \sum_{i=1}^{n}[\pi d_i - k_{i1}\pi_i^2 - k_{i2}(\pi_i^2)\frac{pi_i^2}{\sqrt{\pi^2 + (\frac{\varepsilon_i}{k_{i2}})^2}} - k_{i3}\pi_i^4 - \widehat{p}_i\pi_i tanh\frac{\widehat{p}_i\pi_i}{\delta_i}\\ &\quad + \widehat{p}_i|\pi_i| - p_i|\pi_i| + \frac{\sigma_{i1}}{n_i}\widehat{p}_i\widetilde{p}_i + \frac{\sigma_{i2}}{n_i^2}\widehat{p}_i^3\widetilde{p}_i].\end{aligned} \tag{3.6}$$

According to Lemmas 2.4, 2.5, and 2.8, Eq (3.6) can be scaled as follows:

$$-k_{i2}\frac{\pi_i^2}{\sqrt{\pi^2 + \left(\frac{\varepsilon_i}{k_{i2}}\right)^2}} \leq -k_{i2}\,|\pi_i| + \varepsilon_i, \tag{3.7}$$

$$\pi_i d_i \leq k_{i1}\pi_i^2 + \frac{1}{4k_{i1}}d_i^2, \tag{3.8}$$

$$\hat{p}_i |\pi_i| - \hat{p}_i \pi_i \tanh\left(\frac{\hat{p}_i \pi_i}{\delta_i}\right) \leq k\delta_i. \tag{3.9}$$

In Eq (3.6), the polynomial is transformed, where φ_i and ω_i are constants:

$$\frac{\sigma_{i1}}{n_i^2}\hat{p}_i^3\widetilde{p}_i = \frac{\sigma_{i1}}{n_i}\left(\widetilde{p}_i p_i - \widetilde{p}_i^2\right) + \frac{\sigma_{i1}\varphi_i}{\sqrt{2n_i}}\widetilde{p}_i - \frac{\sigma_{i1}\varphi_i}{\sqrt{2n_i}}\widetilde{p}_i \leq \frac{\sigma_{i1}}{2n_i}p_i^2 + \frac{\sigma_{i1}\varphi_i^2}{4} - \frac{\sigma_{i1}\varphi_i}{\sqrt{2n_i}}\widetilde{p}_i, \tag{3.10}$$

$$\frac{\sigma_{i2}}{n_i^2}\hat{p}_i^3\widetilde{p}_i = \frac{\sigma_{i2}}{n_i^2}\left(-\widetilde{p}_i^4 - 3\widetilde{p}_i^2 p_i^2 + 3p_i\widetilde{p}_i^3 + \widetilde{p}_i p_i^3\right) \leq \frac{\sigma_{i2}}{n_i^2}\left(\frac{1}{4\omega_i^4}\widetilde{p}_i^4 - \frac{1}{4}\widetilde{p}_i^4 + \frac{3\omega_i^{\frac{4}{3}}}{4}\left|p_i^3\right|^{\frac{4}{3}}\right). \tag{3.11}$$

Substituting Eqs (3.7)–(3.11) into the derivative of the Lyapunov function, we obtain:

$$\dot{V}_d \leq \sum_{i=1}^{n}\left[-\sqrt{2}k_{i2}\left(\frac{1}{2}\pi_i^2\right)^{\frac{1}{2}} - 4k_{i3}\left(\frac{1}{2}\pi_i^2\right)^2 - N\right] + M. \tag{3.12}$$

In the equation above, we have:

$$N = \frac{\sigma_{i2}\left(\omega_i^4 - 1\right)}{\omega_i^4 n_i^2}\left(\frac{1}{2}\widetilde{p}_i^2\right)^2 + \frac{\sigma_{i1}\varphi_i}{\sqrt{n_i}}\left(\frac{1}{2}\widetilde{p}_i^2\right)^{\frac{1}{2}}, \tag{3.13}$$

$$M = \sum_{i=1}^{n}\left[\varepsilon_i + \kappa\delta_i + \frac{3\sigma_{i2}\omega_i^{\frac{4}{3}}}{4n_i^2}\left|p_i^3\right|^{\frac{4}{3}} + \frac{\sigma_{i1}\varphi_i^2}{4} + \left(\frac{\sigma_{i1}}{2n_i} + \frac{1}{4k_{i1}}\right)p_i^2\right]. \tag{3.14}$$

By Lemmas 2.6 and 2.7, it can be concluded that when $V_d \geq \sqrt{\frac{M}{t_i}}$, the following holds:

$$\dot{V}_d \leq -t_1 v_d^{\frac{1}{2}} - t_2 v_d^2 + M \leq 0. \tag{3.15}$$

The $t_2 = \min\left\{4k_{i3}, \frac{\sigma_{i2}\left(\omega_i^4-1\right)}{\omega_i^4 n_i^2}\right\}$, $t_1 = \min\left\{\sqrt{2}k_{i2}, \frac{\sigma_{i1}\varphi_i}{\sqrt{n_i}}\right\}$, $i = 1, 2, \ldots, n$.

According to Lemma 2.3, the Lyapunov analysis guarantees that the system exhibits fixed-time convergence, stabilizing within the time bound defined by $T_d \leq \frac{2}{t_1} + \frac{1}{t_2}$. The Lyapunov analysis presented above has demonstrated that π_i converges to a small residual set near the origin within the fixed time T_d. When the state trajectory π_i is effectively stabilized and maintained within a small neighborhood of zero, its time derivative $\dot{\pi}_i$ is also constrained to a bounded small region. Consequently, the convergence of π_i essentially guarantees the convergence of the disturbance estimation error $\tilde{d}_i$. Given that the observer achieves convergence and provides accurate an state estimation within a finite duration, the design of the observer and the controller can be decoupled, as supported by [44, 45].

4. Design of high-reliability cooperative guidance laws

To guarantee the interception of maneuvering targets at a designated relative impact speed, guidance commands are formulated within the LOS channel. Simultaneously, control efforts are exerted in the direction perpendicular to the LOS to ensure that the engagement fulfills the required terminal impact angle specifications. Moreover, a fault-tolerant fallback engagement scheme predicated on fixed-time impact is established. This mechanism ensures that in the event of communication failures, the cooperative guidance logic along the LOS can switch smoothly to the backup mode, thereby ensuring the effective accomplishment of the strike mission.

4.1. Formulation of the high-reliability guidance law for the LOS direction

4.1.1. Guidance law design with relative velocity constraints

Through the synthesis of a control protocol for the LOS subsystem, consensus is achieved regarding the relative velocities and distances among the flight vehicles.

The state-space representation of the LOS subsystem is given by:

$$\begin{cases} \dot{x}_{1i} = x_{2i}, \\ \dot{x}_{2i} = x_{1i}x_{4i}^2 - M_{Ri} + T_{Ri}. \end{cases} \tag{4.1}$$

Drawing upon Lemma 2.1, the sliding mode surface and the consensus protocol ensuring finite-time convergence are formulated as follows:

$$\begin{cases} s_{1i} = x_{2i} - V_{exp} + u_i(c) * t, \\ u_i = -\gamma_1 sig\left[\sum_{l=1}^{n} a_{il}\left(x_{1i} - x_{1l}\right)\right]^{a_1} - \gamma_2 sig\left[\sum_{l=1}^{n} a_{il}\left(x_{2i} - x_{2l}\right)\right]^{\frac{2a_1}{1+a_1}}. \end{cases} \tag{4.2}$$

To alleviate overload saturation in the early phase of guidance, the following adaptive reaching law is designed:

$$\dot{s}_{1i} = g(t, s_{1i}, x_{1i}, T_{rise})(-b_1 sig^{q_1} s_{1i} - b_2 sig^{q_2} s_{1i}). \tag{4.3}$$

In the reaching law, we have $q_1 = \frac{m_1+1}{2} + \frac{m_1-1}{2}\,\mathrm{sgn}(|s_{1i}| - 1)$ and $q_2 = \frac{m_2+1}{2} - \frac{m_2-1}{2}\,\mathrm{sgn}(|s_{1i}| - 1)$, where $m_1 > 1$, $\frac{1}{2} < m_2 < 1$, $b_j > 0$ for $j = 1, 2$, and $\mathrm{sgn}^t(s) = |s|^t\,\mathrm{sgn}(s)$; the function $g(t, s_{1i}, x_{1i}, T_{\mathrm{rise}})$ is specifically given by:

$$g(t, s_{1i}, x_{1i}, T_{\mathrm{rise}}) = \begin{cases} 0, & g_{\mathrm{raw}}(t, s_{1i}, x_{1i}, T_{\mathrm{rise}}) < 0, \\ g_{\mathrm{raw}}(t, s_{1i}, x_{1i}, T_{\mathrm{rise}}), & 0 < g_{\mathrm{raw}}(t, s_{1i}, x_{1i}, T_{\mathrm{rise}}) < g_{\max}, \\ g_{\max}, & g_{\mathrm{raw}}(t, s_{1i}, x_{1i}, T_{\mathrm{rise}}) \geq g_{\max}. \end{cases} \tag{4.4}$$

Here, $g_{\mathrm{raw}}(t, s_{1i}, x_{1i}, T_{\mathrm{rise}}) = t_n(t)(1 + k_p s_n - k_R R_n)$, where $s_n = \dfrac{|s|}{|s|+1}$ and $R_n = \dfrac{|R|}{|R|+1}$; here, $t_n(t)$ is given by

$$t_n(t) = \begin{cases} 0, & t \leq 0, \\ \dfrac{t}{T_{\mathrm{rise}}}, & 0 < t < T_{\mathrm{rise}}, \\ 1, & t \geq T_{\mathrm{rise}}, \end{cases} \tag{4.5}$$

where t is the current time, T_{rise} is the time scale for the gain to reach its full value, t_n is the normalized time factor, and s_n and R_n are the normalized sliding surface and the remaining distance, respectively. The parameters k_p and k_R are gain weights, and $g_{\max}$ denotes the maximum gain.

By equating the time derivative of the sliding surface to the reaching law, we obtain

$$M_{Ri} = x_{1i}x_{4i}^2 + T_{Ri} + u_i - \dot{s}_{1i}. \tag{4.6}$$

Theorem 4.1. In the LOS channel, applying the guidance law given by Eq (4.6) ensures that the flight vehicles strike the maneuvering target at the desired relative impact speed.

Proof. Consider the Lyapunov function candidate defined by:

$$V_{1i} = \frac{1}{2}s_{1i}^2. \tag{4.7}$$

Substituting Eq (4.3) into the derivative of the Lyapunov candidate yields:

$$\begin{aligned}\dot{V}_{1i} &= s_{1i}\dot{s}_{1i} \le s_{1i}g(t, s_{1i}, x_{1i}, T_{rise})\left(-b_1 sgn^{q_1}s_{1i} - b_2 sgn^{q_2}s_{1i}\right)\\ &= g_{max}(t, s_{1i}, x_{1i}, T_{rise})(-b_1 2^{(q_1+1)/2}\left(s_{1i}^2/2\right)^{(q_1+1)/2} - b_2 2^{(q_2+1)/2}\left(s_{1i}^2/2\right)^{(q_2+1)/2})\\ &= g_{max}(t, s_{1i}, x_{1i}, T_{rise})(-b_1\left(2V_{1i}\right)^{(q_1+1)/2} - b_2\left(2V_{1i}\right)^{(q_2+1)/2}).\end{aligned} \tag{4.8}$$

During the convergence of the system, when $|s_{1i}| > 1$, we have $\text{sgn}(|s_{1i}| - 1) = 1$, which gives $q_1 = m_1 > 1$; when $|s_{1i}| = 1$, we have $\text{sgn}(|s_{1i}| - 1) = 0$, which gives $q_1 = (m_1 + 1)/2 > 1$; when $|s_{1i}| < 1$, we have $\text{sgn}(|s_{1i}| - 1) = -1$, which gives $q_1 = 1$. Hence $q_1 > 1$; and similarly, one obtains $q_2 < 1$.

Therefore, when V_{1i} is sufficiently small (approaching zero), the term with the smallest exponent dominates the decay rate, and the dynamics can be approximated as follows:

$$\dot{V}_{1i} \le -b_2 g_{max}(t, s_{1i}, x_{1i}, T_{rise})\left(2V_{1i}\right)^{(q_2+1)/2}. \tag{4.9}$$

Let $\frac{q_2+1}{2} = \gamma_1$ and $b_2 2^{\gamma_1} g_{\max}(t, s_{1i}, x_{1i}, T_{\text{rise}}) = C$. We then have

$$\dot{V}_{1i} \le -cV_{1i}^{\gamma_1}. \tag{4.10}$$

According to Lemma 2.2, it can be concluded that finite-time convergence can be achieved when $0 < q_2 < 1$ [46].

Next, substituting the control input into the LOS direction subsystem gives

$$\begin{cases}\dot{x}_{1i} = x_{2i},\\ \dot{x}_{2i} = -u_i + \dot{s}_{0i}.\end{cases} \tag{4.11}$$

The dynamic variable $\dot{s}_{0i}$ associated with the LOS direction is guaranteed to converge to zero within a finite duration. Consequently, once the sliding mode surface stabilizes, the aforementioned second-order system conforms to the criteria set forth in Definition 2.1, thereby ensuring that the LOS subsystem achieves a consensus in finite time.

4.1.2. Design of the fault-tolerant backup guidance law

To facilitate the synchronized interception of a maneuvering target by the flight vehicles, an accurate estimation of the remaining flight time is a prerequisite. Accordingly, the time-to-go, denoted $t_{go,i}$, is introduced. Its specific mathematical expression is formulated as follows:

$$t_{go,i} = -\frac{R_i}{\dot{R}_i}. \tag{4.12}$$

In cooperative guidance frameworks, t_{go} is frequently utilized to denote the estimated time-to-go. Although this approximation may introduce estimation discrepancies during the initial engagement phase, the error decays rapidly and asymptotically approaches zero as the distance to the target decreases. Consequently, the impact of the initial estimation inaccuracies on the overall guidance performance is negligible. Taking the time derivative of $t_{go,i}$ yields

$$\dot{t}_{go,i} = -\frac{\dot{R}_i^2 - R_i\ddot{R}_i}{\dot{R}_i^2} = -\frac{x_{2i}^2 - x_{1i}\dot{x}_{2i}}{x_{2i}^2} = -1 + \frac{x_{1i}}{x_{2i}^2}(x_{1i}x_{4i}^2 - M_{Ri} + T_{Ri}). \tag{4.13}$$

Consequently, the total flight duration is determined by $T_{f,i} = t + t_{go,i}$. In accordance with [47], the sliding mode surface is constructed as follows:

$$s_{1i} = T_{f,i} - T_d. \tag{4.14}$$

Here, $T_d = t_{go,\text{end}} + t_{\text{end}} - t_n$ defines the desired total flight time, where $t_{go,\text{end}}$ and t_{end} signify the estimated time-to-go and the absolute time at the moment of guidance law switching, respectively. To ensure the terminal engagement occurs with an impact velocity surpassing the nominal specification, the intended flight duration in the second phase is curtailed by the subtraction of t_n. The time derivative of the sliding surface is subsequently derived as follows:

$$\dot{s}_{1i} = 1 + \dot{t}_{go,i} = \frac{x_{1i}}{x_{2i}^2}(x_{1i}x_{4i}^2 - M_{Ri} + T_{Ri}). \tag{4.15}$$

The approach law's design is as follows:

$$\dot{s}_{2i} = g(t, s_{2i}, x_{1i}, T_{rise})(-b_1 sig^{q_1} s_{2i} - b_2 sig^{q_2} s_{2i}). \tag{4.16}$$

Accordingly, the fault-tolerant backup guidance law for the LOS channel is formulated as:

$$M_{Ri} = x_{1i}x_{4i}^2 + T_{Ri} - \frac{x_{1i}}{x_{2i}^2}\dot{s}_{1i}. \tag{4.17}$$

Prior to the onset of a communication fault, the cooperative control input along the LOS, derived subject to the relative impact velocity constraint, is denoted M_{R,i,t_d}, where t_d signifies the epoch of communication failure. Following the fault, the control input is designated as $M_{R,i,t}$. To alleviate the actuator's burden, a transition strategy is used to smooth the control inputs across the failure boundary, with the specific smoothing mechanism defined by

$$M_{R,i,t} = M_{R,i,t_d} + (M_{R,i,t} - M_{R,i,t_d})\frac{e^{t-t_d} - e^{t_d-t}}{e^{t-t_d} + e^{t_d-t}}. \tag{4.18}$$

4.2. Formulation of the guidance law subject to LOS normal angle constraints

The state-space dynamics corresponding to the subsystem normal to the LOS are described by:

$$\begin{cases} \dot{x}_{3i} = x_{4i}, \\ \dot{x}_{4i} = -\dfrac{2x_{2i}x_{4i}}{x_{1i}} - \dfrac{M_{qi}}{x_{1i}} + \dfrac{T_{qi}}{x_{1i}}. \end{cases} \tag{4.19}$$

The sliding surface is constructed as follows [48]:

$$s_{3i} = x_{4i} - \frac{2n_1\dot{R}_i}{R_i}x_{3i} + \frac{k_s}{R_i^{n_1}}x_{3i}. \tag{4.20}$$

By leveraging the reciprocal property of the relative distance R_i, the guidance law is given time-varying convergence characteristics. During the initial interception phase (where R_i is large), the relatively small gain helps prevent control input saturation. Conversely, in the terminal phase (as $R_i \to 0$), the gain increases drastically as the distance decreases. This provides a strong driving force for convergence, ensuring that the LOS angle constraints are satisfied with high precision at the instant of impact. The reaching law is formulated as follows:

$$\dot{s}_{3i} = g\left(t, s_{3i}, x_{1i}, T_{rise}\right)\left(-b_1 sig^{q_1} s_{3i} - b_2 sig^{q_2} s_{3i}\right). \tag{4.21}$$

Synthesizing Eqs (4.20) and (4.21), the control input aligned with the normal direction of the LOS is derived as follows:

$$M_{qi} = x_{1i}(-\frac{2x_{2i}x_{4i}}{x_{1i}} + \frac{T_{qi}}{x_{1i}} - \frac{2n_1\ddot{R}_i}{R_i}x_{3i} + \frac{2n_1\dot{R}_i^2}{R_i^2}x_{3i} - \frac{2n_1\dot{R}_i}{R_i}x_{4i} + \frac{k_s}{R_i^{n_1}}x_{4i} - \frac{n_1\dot{R}_i k_s}{R_i^{n_1+1}}x_{3i} - \dot{s}_{3i}). \tag{4.22}$$

The proof of convergence for the LOS normal sliding surface is omitted for brevity, as it follows a procedure identical to that of the LOS direction.

Theorem 4.2. For the subsystem governing the dynamics normal to the LOS, if the guidance law is implemented according to Eq (4.22), the system's states are guaranteed to converge, thereby ensuring that the flight vehicles intercept the target at the prescribed impact angle.

Proof. Once the system's trajectories reach the sliding manifold, the relationship $x_{4i} = \frac{2n_1\dot{R}_i}{R_i}\, x_{3i} - \frac{k_s}{R_i^{n_1}}\, x_{3i}$ is established. To analyze the stability, a Lyapunov function candidate is constructed as follows:

$$V_{2i} = \frac{1}{2}x_{3i}^2. \tag{4.23}$$

By taking the derivative, we obtain:

$$\begin{aligned} \dot{V}_{2i} = x_{3i}\dot{x}_{3i} &= x_{3i}\left(\frac{2n_1\dot{R}_i}{R_i}x_{3i} - \frac{k_s}{R_i^{n_1}}x_{3i}\right) \\ &= \frac{2n_1\dot{R}_i}{R_i}x_{3i}^2 - \frac{k_s}{R_i^{n_1}}x_{3i}^2. \end{aligned} \tag{4.24}$$

Considering that $\dot{R}_i$ denotes the relative closing velocity, which remains strictly negative ($\dot{R}_i < 0$) as the vehicle closes in on the target, the asymptotic stability of the system is secured as long as the

design parameters are chosen to satisfy $n_1 > 0$ and $k_s > 0$. The parameter k_s determines the baseline convergence rate of the system. A larger value of k_s increases the magnitude of the negative definite term in the Lyapunov derivative $\dot{V}_{2i}$, thereby accelerating the convergence of the LOS angle error x_{3i}. However, an excessively large k_s may lead to actuator saturation, potentially compromising the stability of the guidance process.

4.3. Simulation parameter configuration

To validate the effectiveness of the proposed method, numerical simulations are conducted. The initial conditions for the flight vehicles and the target adopted in the subsequent verification are listed in Table 1.

Table 1. Initial conditions of the flight vehicle and target.

	M1	M2	M3	M4	Target
Position (m)	(-1000,0)	(0,0)	(1000,0)	(2000,0)	(10000,10000)
V (m/s)	470	450	400	480	200
$\theta_{M/T}$ (°)	35	45	45	55	-10
q_{exp} (°)	30	40	50	60	/

The specific parameters governing the guidance law and the observer are detailed in Table 2.

Table 2. Guidance law and observer parameters.

Parameter	Value	Parameter	Value	Parameter	Value	Parameter	Value
m_1	$\frac{9}{7}$	m_2	$\frac{7}{9}$	b_1	1.5	b_2	1.5
T_{rise}	10	g_{max}	1	k_p	0.3	a	0.88
k_R	0.2	$\frac{\sigma_{i1}}{n_i}$	10	n_1	0.8	$\frac{\sigma_{i2}}{n_i^2}$	0.01
k_s	50	ε_i	0.5	k_{i1}	8	δ_i	0.5
k_{i2}	0.5	k_{i3}	0.5				

The acceleration saturation for each flight vehicle is configured at $30g$. The maneuvering target executes a serpentine motion, with its acceleration profile defined as $a_T = a_{Tr} = 3g\sin(0.6t) + 0.5k_{\text{rand}}g$, where k_{rand} represents a random variable within [0, 1], where $0.5k_{rand}g$ represents the simulated external disturbance. Figure 2 illustrates the communication topology used in this study.

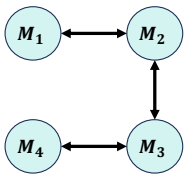

Figure 2. Communication topology.

5. Simulation results

To assess the efficacy of the proposed guidance scheme in intercepting maneuvering targets subject to prescribed constraints, numerical simulations are conducted across three distinct scenarios:

Cooperative guidance within an ideal environment, adaptive cooperative guidance under ideal conditions, and adaptive high-reliability cooperative guidance subjected to communication disruptions. Furthermore, Monte Carlo simulations are performed to rigorously validate the robustness and adaptability of the developed guidance law.

5.1. Cooperative guidance under ideal conditions

To validate the superiority of the proposed adaptive reaching law, a comparative simulation is conducted under ideal conditions where the adaptive term $g(t, s_i, x_{1i}, T_{\text{rise}})$ is omitted, utilizing only the conventional double power reaching law. The resulting performance of the cooperative guidance system is illustrated in Figure 3. As shown by Figure 3(a), (d), and (e), the relative distances and remaining flight times of all vehicles rapidly achieve a consensus, ensuring the simultaneous interception of the maneuvering target. The NDO estimation results presented in Figure 3(b), (c) demonstrate that the target acceleration along the LOS is accurately estimated; while the normal acceleration estimate exhibits initial transient deviations, it converges rapidly to accurately reconstruct the external disturbance induced by the target's maneuvers. However, the enforcement of the relative impact velocity constraint compels vehicles with lower initial speeds to accelerate aggressively. As depicted in Figure 3(f), this leads to actuator saturation during the initial phase, which poses a potential challenge to the stability of the guidance process. Nevertheless, as shown in Figure 3(g)–(i), both the relative impact velocities and LOS angles converge precisely to their desired values, ensuring that target interception satisfies the prescribed terminal angle and velocity constraints.

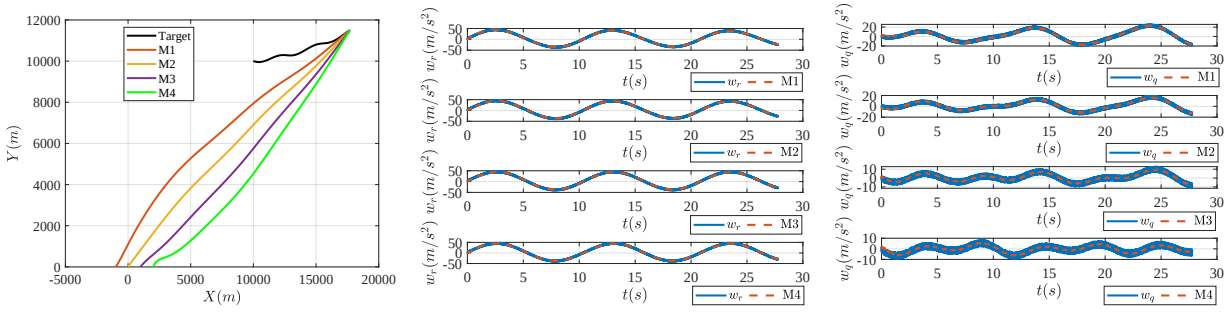

(a) Interception trajectory (b) W_r Observation results (c) W_q Observation results

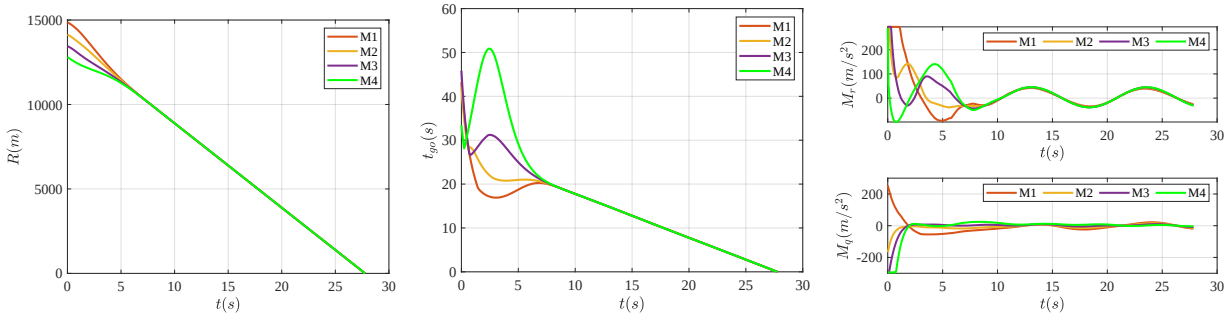

(d) Relative distance (e) Remaining flight time (f) Acceleration

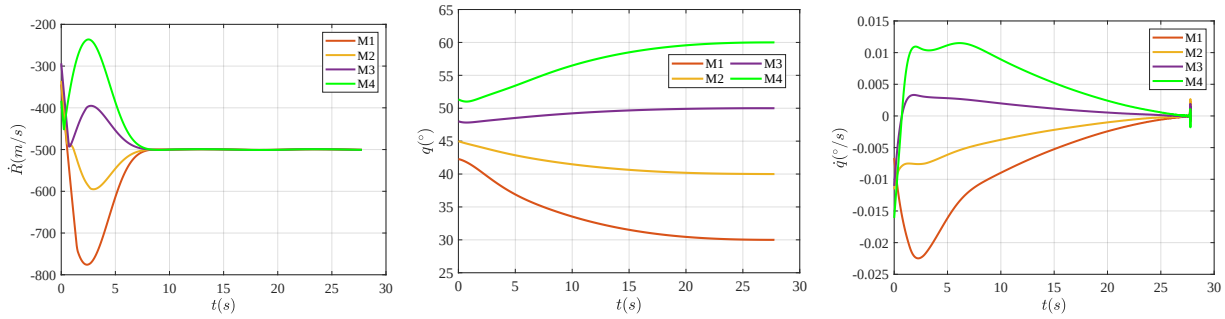

(g) Relative velocity (h) LOS inclination angle curve (i) LOS inclination angle rate

Figure 3. Cooperative guidance simulation results under ideal conditions.

The simulation results under ideal conditions, as detailed in Table 3, indicate that the flight vehicles achieve rapid convergence to the desired relative impact velocity and terminal angles against the maneuvering target. Quantitatively, the maximum miss distance is recorded at 0.49366 m, with the peak relative velocity error across the formation restricted to 0.59918 m/s. Moreover, the tracking errors for the designated impact angles are virtually non-existent. These outcomes substantiate that the proposed guidance scheme successfully executes cooperative interception while rigorously satisfying the constraints on the relative impact velocity and terminal angles.

Table 3. Simulation test outcomes for cooperative guidance in the absence of communication interference.

	Miss distance (m)	Error in $\dot{R}$ (m/s)	Error in q (°)
M1	0.49104	0.58755	7.41E-04
M2	0.49295	0.59275	4.07E-04
M3	0.49354	0.59697	4.31E-04
M4	0.49366	0.59918	7.30E-04

5.2. Adaptive cooperative guidance under ideal conditions

Acknowledging that exclusive reliance on the double power reaching law for cooperative guidance induces acceleration saturation during the initial engagement phase—thereby compromising the system's stability—an adaptive term, denoted $g(t, s_{3i}, x_{1i}, T_{\text{rise}})$, is integrated into the reaching law to synthesize an adaptive cooperative guidance strategy. As illustrated in Figure 4(a), (d), and (e), the states of the flight vehicles rapidly achieve consensus, facilitating coordinated engagement of the maneuvering target. Furthermore, Figure 4(b), (c) demonstrates that the observer maintains the capability to estimate the target's uncertainties with high speed and precision. Crucially, the incorporation of the adaptive term effectively eliminates the acceleration saturation observed in Figure 4(f), resulting in a significantly smoother control profile. Finally, Figure 4(g)–(i) confirms that the vehicles successfully intercept the target while strictly satisfying the prescribed impact angle and velocity constraints.

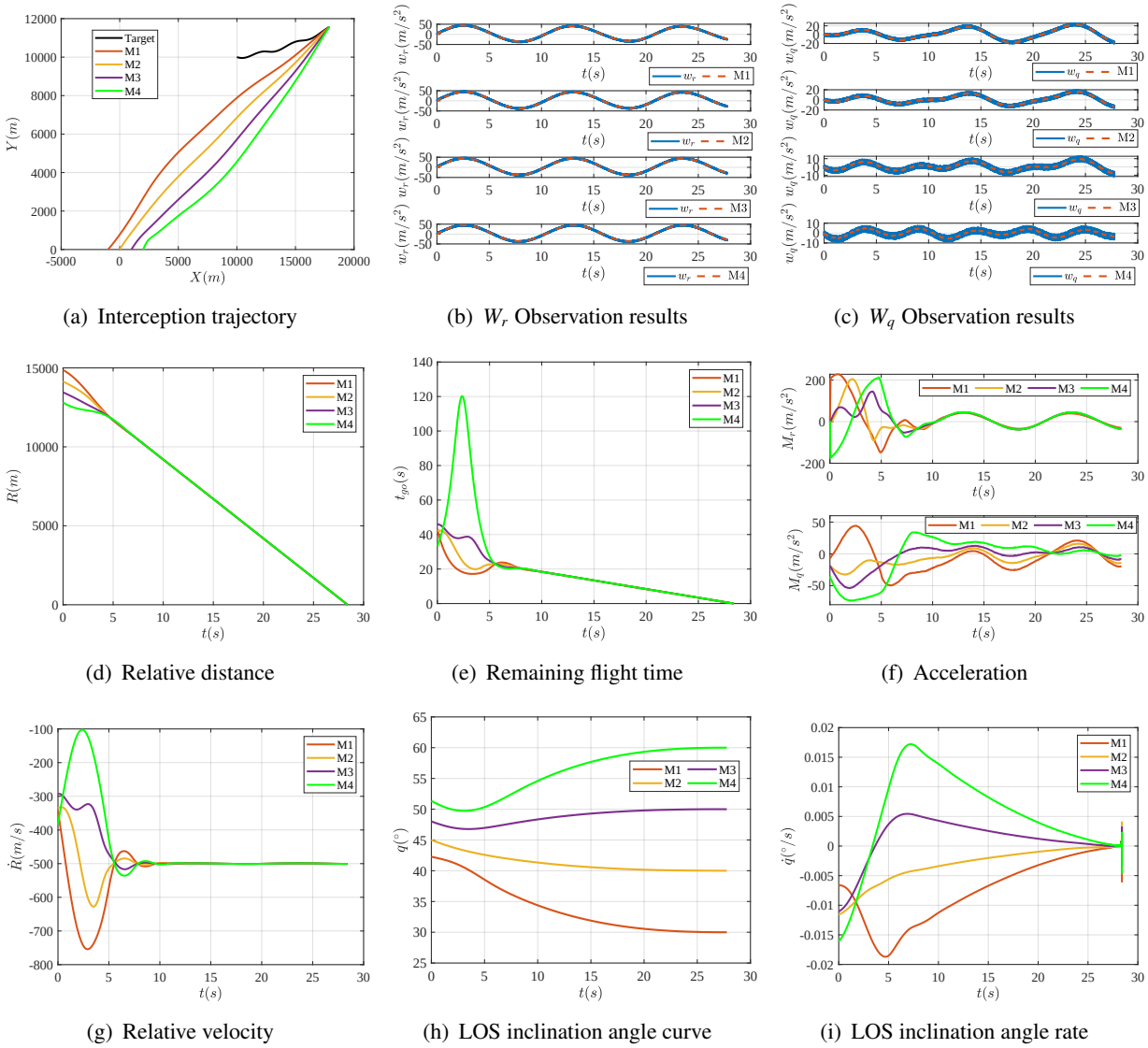

(a) Interception trajectory (b) W_r Observation results (c) W_q Observation results

(d) Relative distance (e) Remaining flight time (f) Acceleration

(g) Relative velocity (h) LOS inclination angle curve (i) LOS inclination angle rate

Figure 4. Adaptive cooperative guidance simulation results under ideal conditions.

Table 4. Adaptive cooperative guidance simulation test results under ideal conditions.

	Miss distance (m)	Error in $\dot{R}$ (m/s)	Error in q (°)
M1	0.4589	0.7615	1.76E-04
M2	0.4599	0.7595	2.84E-04
M3	0.4591	0.7557	2.76E-04
M4	0.4583	0.7538	2.61E-04

The quantitative results provided in Table 4 under ideal conditions confirm that the flight vehicles efficiently adjust their states to meet the required relative impact velocity and impact angle constraints for intercepting the maneuvering target. Specifically, the maximum recorded miss distance is 0.4599 m, while the peak discrepancy in relative velocity among the four units is limited to merely 0.7615 m/s. Furthermore, deviations from the desired impact angles are minimal. Consequently, these findings

validate that the guidance law proposed in this study effectively achieves cooperative engagement of maneuvering targets while strictly adhering to the prescribed relative impact velocity and terminal angle specifications.

5.3. Adaptive cooperative guidance under communication interruptions

Under communication interruptions, the conventional closed-loop cooperative mechanism fails, which directly degrades the cooperative performance of the flight vehicles and may even cause mission failure. Therefore, in this subsection an open-loop cooperative strategy with a fixed time of impact is designed, in which the closed-loop cooperative mechanism is switched to a fixed-time engagement scheme once communication is interrupted.

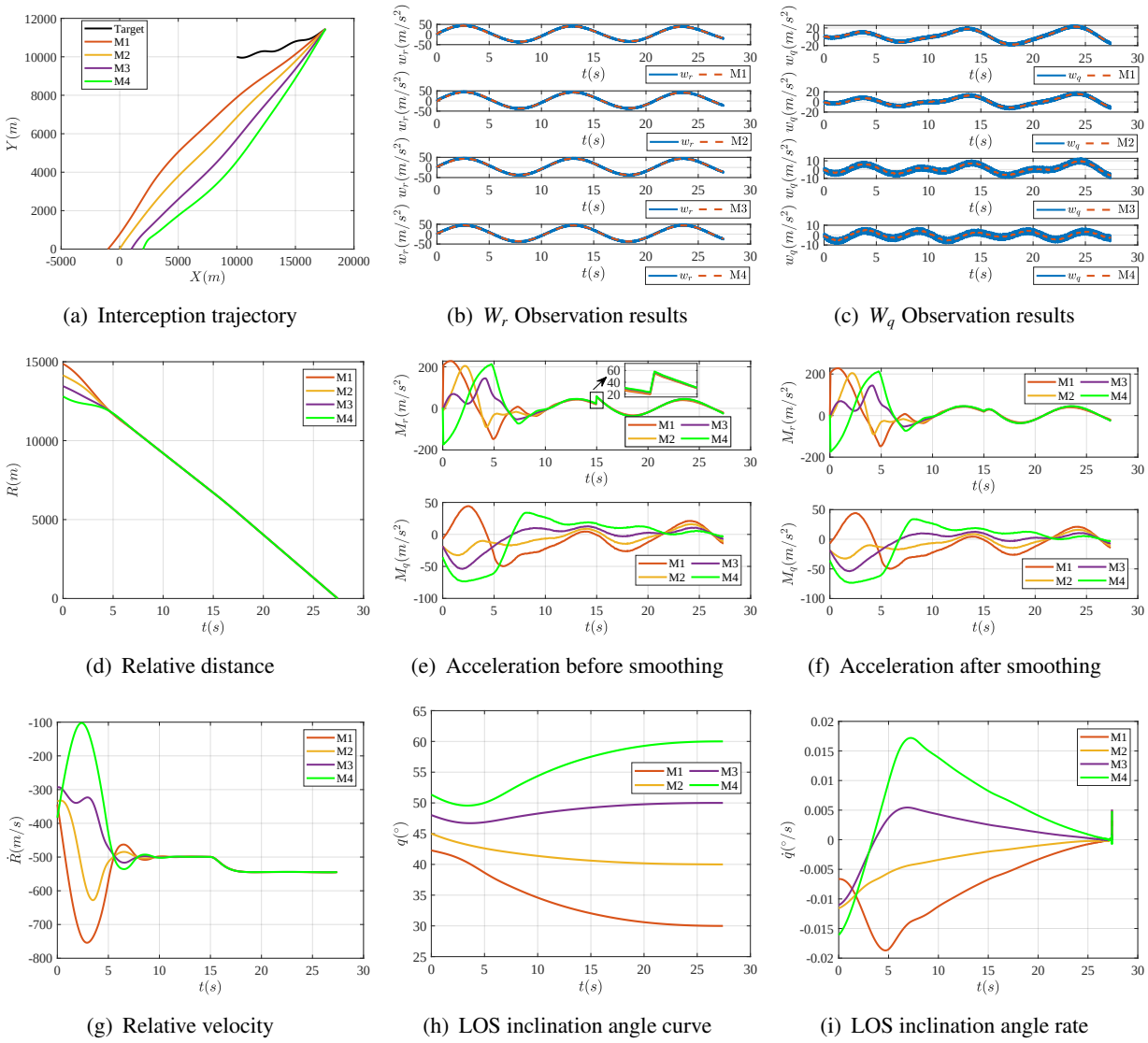

(a) Interception trajectory (b) W_r Observation results (c) W_q Observation results

(d) Relative distance (e) Acceleration before smoothing (f) Acceleration after smoothing

(g) Relative velocity (h) LOS inclination angle curve (i) LOS inclination angle rate

Figure 5. Adaptive cooperative guidance simulation results under communication interruptions.

The simulation results corresponding to the adaptive cooperative guidance scenario under

communication interruption are presented in Figure 5. As evidenced by Figure 5(a), (d), the proposed guidance law maintains the capability to achieve cooperative engagement against the maneuvering target, even in the event of a communication failure. Furthermore, Figure 5(b), (c) indicates that the observer retains the ability to rapidly and accurately estimate the external disturbances induced by the target's acceleration. As depicted in Figure 5(e), (f), an abrupt transition in the control strategy results in acceleration discontinuities, imposing excessive mechanical stress on the actuators. Conversely, the implementation of the proposed smoothing strategy ensures a seamless transition between control modes, thereby effectively enhancing the stability of the guidance process. Moreover, Figure 5(h), (i) demonstrates the robust terminal constraint capability of the proposed guidance law, ensuring consistent system convergence to the desired impact angle. Given that the impact time for the second stage is defined as $T_d = t_{go,\text{end}} + t_{\text{end}} - t_n$, which is shorter than the cooperative engagement under the nominal relative impact velocity constraint, the relative impact velocity is further augmented, as shown in Figure 5(g). Consequently, the switching of the control strategy does not compromise the impact kinetic energy.

The primary motivation for this strategy switching is to sustain cooperative functionality during communication outages. By leveraging a fixed-time open-loop coordination scheme, the flight vehicles can achieve coordinated engagement independent of real-time communication feedback. This approach not only guarantees mission continuity under communication constraints but also effectively mitigates the adverse effects associated with communication delays and packet loss. Through this strategic switching mechanism, the vehicles remain capable of efficiently accomplishing their missions within complex operational environments.

As indicated in Table 5, all flight vehicles successfully intercept the maneuvering target while strictly adhering to the prescribed impact angle constraints. The maximum recorded miss distance is limited to 0.5708 m, which fully satisfies engineering precision requirements. Given that the designated flight duration for the second stage is truncated relative to the nominal cooperative engagement timeline, the vehicles are compelled to accelerate to achieve an expedited interception. Consequently, the uniform interception time for all units is observed at 27.414 s, confirming that the strike mission remains viable even under conditions of communication failure. Thus, the proposed adaptive cooperative guidance law not only ensures compliance with impact kinetic energy constraints but also significantly enhances the overall stability and reliability of the cooperative engagement system.

Table 5. Adaptive cooperative guidance simulation test results under communication interruptions.

	Miss distance (m)	Error in $\dot{R}$ (m)	Error in q (°)	Interception Time (s)
M1	0.5708	44.1215	1.92E-04	27.414
M2	0.5708	43.9299	1.91E-04	27.414
M3	0.5659	43.8037	1.71E-04	27.414
M4	0.5632	43.7335	1.49E-04	27.414

To further highlight the superiority of the proposed guidance law, a comparison is conducted with the sliding surface and reaching law for the LOS normal component presented in [4]. The parameter configurations are kept consistent with the original study, and this method is denoted as GL-1.

It can be observed from Figure 6(a), (c) that although the LOS angle of the vehicle can rapidly converge to the desired value and achieve precise target interception, the results in Figure 6(b) indicate that this rapid convergence significantly increases the normal acceleration. This not only increases energy consumption but also directly affects the stability of the guidance process.

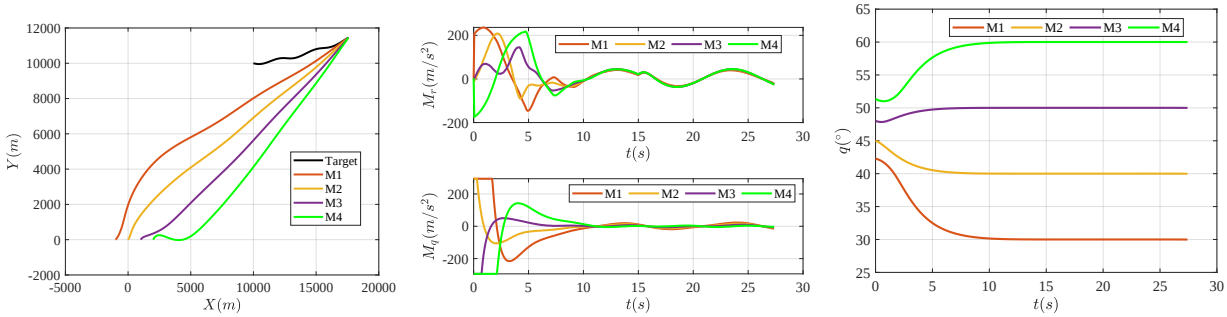

(a) Interception trajectory (b) Acceleration after smoothing (c) LOS inclination angle curve

Figure 6. Simulation results of the GL-1 guidance law under communication interruptions.

As shown in Table 6, the simulation results for GL-1 indicate a significant increase in the LOS angle error. The rapid convergence of the LOS angle does not enhance the constraint capability of the guidance law; instead, it imposes a heavy burden on the actuators. In contrast, the proposed guidance law achieves a better balance between acceleration magnitude and terminal angle constraint capability, demonstrating superior stability.

Table 6. Test results of the GL-1 guidance law under communication interruptions.

	Miss distance (m)	Error in $\dot{R}$ (m)	Error in q (°)	Interception time (s)
M1	0.63232	44.1615	1.81E-02	27.413
M2	0.63222	43.9510	2.44E-02	27.413
M3	0.62738	43.8185	1.65E-02	27.413
M4	0.62467	43.7543	7.98E-03	27.413

5.4. Monte Carlo simulation test

To assess the adaptability and robustness of the guidance strategy proposed herein, Monte Carlo simulations are performed on the fault-tolerant control framework, particularly under scenarios involving intense communication interference. The verification procedure is divided into two distinct stages.

(1) Assessment of the guidance law's adaptability across varying launch conditions, with fixed initial target parameters.

To assess robustness, 500 Monte Carlo simulations are performed under randomized launch conditions. Specifically, the initial deviations for position and velocity are constrained within $[-100, 100]$ m and $[-10, 10]$ m/s, respectively. For angular parameters, both the initial flight path angle's error and the expected LOS angle's error are bounded between $-5°$ and $5°$. All the aforementioned initial errors are assumed to obey a uniform distribution. Furthermore, measurement uncertainties are modeled by injecting zero-mean Gaussian noise into $\dot{R}$ and the LOS angular rate

$\dot{q}$, with the variances set to 1 m/s and 0.005 rad/s, respectively. The simulation terminates once the relative distance $R < 1$ m and $\dot{R} > 0$. The corresponding statistical results are depicted in Figure 7.

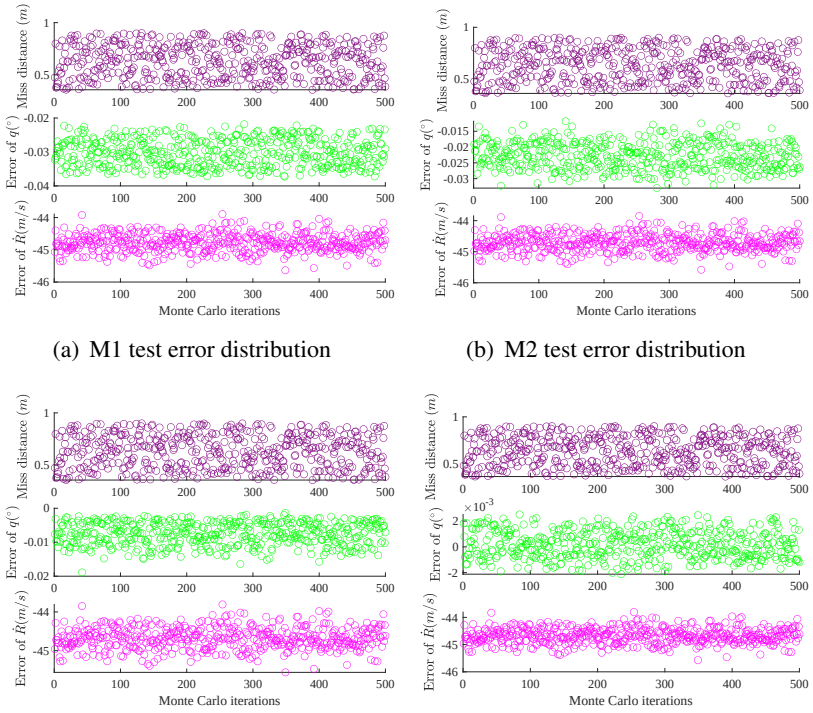

(a) M1 test error distribution

(b) M2 test error distribution

(c) M3 test error distribution

(d) M4 test error distribution

Figure 7. First set of Monte Carlo simulation results.

Figure 7 illustrates the Monte Carlo simulation results for the flight vehicles under varying launch conditions, with the target's initial parameters held fixed. Observations from Figure 7(a)–(d) indicate that, despite variations in the initial launch geometry, all four flight vehicles successfully engage the maneuvering target while strictly satisfying the terminal angular constraints and maintaining minimal miss distances. Specifically, the maximum terminal angle deviation is constrained to less than 0.04°, and the relative impact velocity is augmented by 45 m/s. This performance ensures accurate cooperative engagement while simultaneously guaranteeing sufficient terminal kinetic energy.

(2) The initial parameters of the flight vehicles are fixed to verify the robustness of the guidance law against varying initial conditions of the hostile target.

For the maneuvering target, the initial perturbations regarding the position, velocity, and flight path angle are assigned the same error magnitudes as those defined for the flight vehicles. The requirement to intercept the target at the prescribed terminal angle remains unchanged. Under these configurations, 500 Monte Carlo runs are carried out, as illustrated in Figure 8.

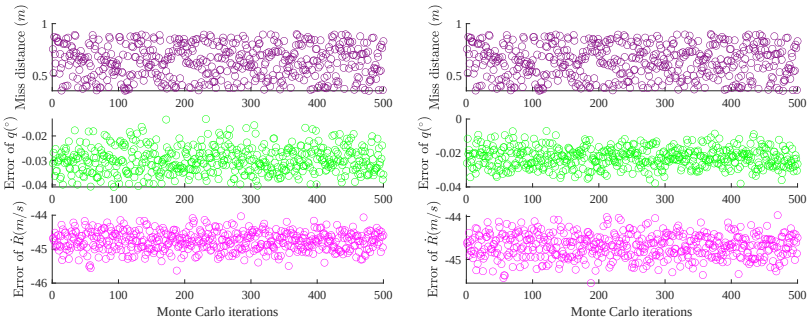

(a) M1 test error distribution

(b) M2 test error distribution

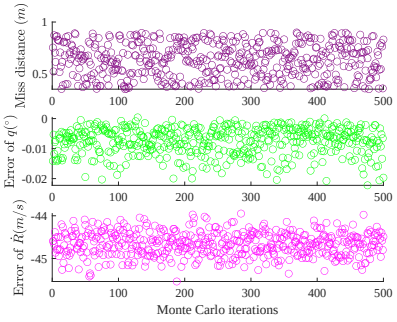

(c) M3 test error distribution

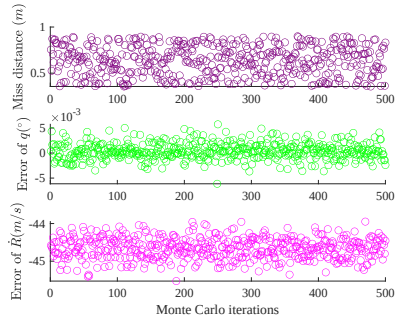

(d) M4 test error distribution

Figure 8. Second set of Monte Carlo simulation results.

Figure 8 illustrates the Monte Carlo simulation results for the flight vehicles configured with fixed launch parameters, engaging maneuvering targets subject to varying initial conditions. As shown in Figure 8(a)–(d), despite the variations in the target's initial state, all four flight vehicles successfully intercept the target while maintaining identical launch parameters, achieving minimal miss distances and terminal impact angle errors. No interception failures were recorded, and both the terminal angle's accuracy and the relative impact kinetic energy consistently satisfy the engineering requirements. These results substantiate the robust adaptability and reliability of the proposed guidance law.

The comprehensive analysis of simulation data—spanning ideal scenarios, interference-laden environments, and Monte Carlo engagement tests—unequivocally establishes the superiority of the proposed guidance framework. Moreover, by enforcing simultaneous constraints on the impact velocity and attack angle, the designed guidance law not only substantially reinforces the strike lethality of the flight vehicles but also improves the robustness and adaptability of the entire guidance sequence.

6. Conclusions

In the context of modern electronic countermeasures, this paper proposes an adaptive high-reliability cooperative guidance law to address the challenge of communication link interruptions. A fault-tolerant backup guidance scheme is designed, incorporating a control smoothing mechanism to ensure seamless transitions during strategy switching.

Simulation results across various scenarios, including ideal combat environments and communication outages, demonstrate that the proposed guidance law achieves the cooperative interception of maneuvering targets with the desired relative impact kinetic energy and impact angles.

The introduction of an adaptive term effectively eliminates acceleration saturation and enhances the stability of the guidance process. Furthermore, in the event of a communication link failure, the system can rapidly transition to the fault-tolerant backup option to execute fixed-time open-loop cooperative engagement. This capability significantly improves the reliability of the guidance process and ensures successful mission execution. Monte Carlo simulations further substantiate the superior adaptability and robustness of the proposed method, and both the theoretical analysis and the numerical validation fully confirm the effectiveness and superiority of the guidance law presented in this study.

Multi vehicle cooperative guidance represents a pivotal technology for enhancing strike capabilities. Although this study accounts for external communication interference and proposes a fault-tolerant guidance law to mitigate environmental impacts, the minimum separation distance between vehicles may still decrease significantly during cooperation. Consequently, the internal safety of the formation (collision avoidance) during the cooperative guidance process remains an area requiring further improvement.

Author contributions

Zewei Liu: Methodology, software, validation, data curation, writing – original draft, and visualization; Zhanpeng Gao: Conceptualization, methodology, formal analysis, writing – review, editing, and supervision. All authors have read and approved the final version of the manuscript for publication.

Use of Generative-AI tools declaration

The authors declare that they have not used artificial intelligence tools in the creation of this article.

Acknowledgments

This work was supported by the National Natural Science Foundation of China (grant numbers 62203191), the National Defence Key Laboratory of Science and Technology (grant numbers 2022JCJQLB06105), the Basic Science (Natural Science) Research Projects in Higher Education Institutions (grant numbers 22KJB590001), the China Postdoctoral Science Foundation (grant numbers 2024M754148), and the Postdoctoral Fellowship Program (Grade B) of China Postdoctoral Science Foundation (grant numbers GZB20240980).

Conflict of interest

The authors declare that they have no known competing financial interests or personal relationships that could have appeared to influence the work reported in this paper.

References

1. J. Yu, X. Dong, Q. Li, Z. Ren, J. Lv, Cooperative guidance strategy for multiple hypersonic gliding vehicles system, *Chin. J. Aeronaut.*, **33** (2020), 990–1005. https://doi.org/10.1016/j.cja.2019.12.003

2. S. Liu, B. Yan, T. Zhang, P. Dai, R. Liu, J. Yan, Three-dimensional cooperative guidance law for intercepting hypersonic targets, *Aerosp. Sci. Technol.*, **129** (2022), 107815. https://doi.org/10.1016/j.ast.2022.107815

3. S. Zhao, R. Zhou, Cooperative guidance for multimissile salvo attack, *Chin. J. Aeronaut.*, **21** (2008), 533–539. https://doi.org/10.1016/S1000-9361(08)60171-5

4. H. You, X. Chang, J. Zhao, S. Wang, Y. Zhang, Three-dimensional impact-angle-constrained cooperative guidance strategy against maneuvering target, *ISA Trans.*, **138** (2023), 262–280. https://doi.org/10.1016/j.isatra.2023.02.030

5. Z. Wang, W. Fu, Y. Fang, S. Zhu, Z. Wu, M. Wang, Prescribed-time cooperative guidance law against maneuvering target based on leader-following strategy, *ISA Trans.*, **129** (2022), 257–270. https://doi.org/10.1016/j.isatra.2022.02.043

6. Y. Zhan, S. Li, D. Zhou, Time-to-go based three-dimensional multi-missile spatio-temporal cooperative guidance law: A novel approach for maneuvering target interception, *ISA Trans.*, **149** (2024), 178–195. https://doi.org/10.1016/j.isatra.2024.04.017

7. H. You, X. Chang, J. Zhao, S. Wang, Y. Zhang, Three-dimensional impact-angle-constrained fixed-time cooperative guidance algorithm with adjustable impact time, *Aerosp. Sci. Technol.*, **141** (2023), 108574. https://doi.org/10.1016/j.ast.2023.108574

8. X. Wang, X. Lu, Three-dimensional impact angle constrained distributed guidance law design for cooperative attacks, *ISA Trans.*, **73** (2018), 79–90. https://doi.org/10.1016/j.isatra.2017.12.009

9. Z. Chen, W. Chen, X. Liu, J. Cheng, Three-dimensional fixed-time robust cooperative guidance law for simultaneous attack with impact angle constraint, *Aerosp. Sci. Technol.*, **110** (2021), 106523. https://doi.org/10.1016/j.ast.2021.106523

10. Y. Xiong, J. Li, C. Hu, L. Tan, Three-dimensional cooperative guidance strategy for heterogeneous vehicles without prior communication topology establishment, *Aerosp. Sci. Technol.*, **161** (2025), 110095. https://doi.org/10.1016/j.ast.2025.110095

11. H. Li, Y. Deng, Y. Cai, Three-dimensional cooperative interception guidance law with impact time constraint, *Proc. Inst. Mech. Eng. Part G J. Aerosp. Eng.*, **236** (2022), 191–201. http://dx.doi.org/10.1177/09544100211010524

12. C. Wang, X. Ding, J. Wang, J. Shan, A robust three-dimensional cooperative guidance law against maneuvering target, *J. Franklin Inst.*, **357** (2020), 5735–5752. https://doi.org/10.1016/j.jfranklin.2020.03.007

13. Z. Wang, Y. Fang, W. Fu, W. Ma, M. Wang, Prescribed-time cooperative guidance law against manoeuvring target with input saturation, *Int. J. Control*, **96** (2023), 1177–1189. https://doi.org/10.1080/00207179.2022.2033850

14. Z. He, S. Fan, J. Wang, P. Wang, Distributed observer-based fixed-time cooperative guidance law against maneuvering target, *Int. J. Robust Nonlinear Control*, **34** (2024), 27–53. https://doi.org/10.1002/rnc.6959

15. Y. Zhan, S. Li, D. Zhou, Time-to-go based three-dimensional multi-missile spatio-temporal cooperative guidance law: A novel approach for maneuvering target interception, *ISA Trans.*, **149** (2024), 178–195. https://doi.org/10.1016/j.isatra.2024.04.017

16. F. Dong, X. Zhang, P. Tan, Non-singular terminal sliding mode cooperative guidance law under impact angle constraint, *J. Franklin Inst.*, **361** (2024), 107079. https://doi.org/10.1016/j.jfranklin.2024.107079
17. M. Guo, F. Yang, G. Xia, K. Liu, Three-dimensional free-will arbitrary time cooperative guidance law against moving target, *J. Franklin Inst.*, **361** (2024), 106969. https://doi.org/10.1016/j.jfranklin.2024.106969
18. G. Li, Q. Li, Y. Wu, P. Xu, J. Liu, Leader-following cooperative guidance law with specified impact time, *Sci. China Technol. Sci.*, **63** (2020), 2349–2356. https://doi.org/10.1007/s11431-020-1669-3
19. P. Zhang, X. Zhang, Multiple missiles fixed-time cooperative guidance without measuring radial velocity for maneuvering targets interception, *ISA Trans.*, **126** (2022), 388–397. https://doi.org/10.1016/j.isatra.2021.07.023
20. Z. Wang, W. Fu, Y. Fang, S. Zhu, Z. Wu, M. Wang, Prescribed-time cooperative guidance law against maneuvering target based on leader-following strategy, *ISA Trans.*, **129** (2022), 257–270. https://doi.org/10.1016/j.isatra.2022.02.043
21. S. Liu, B. Yan, T. Zhang, P. Dai, R. Liu, J. Yan, Three-dimensional cooperative guidance law for intercepting hypersonic targets, *Aerosp. Sci. Technol.*, **129** (2022), 107815. https://doi.org/10.1016/j.ast.2022.107815
22. Z. Chen, X. Liu, W. Chen, Three-dimensional event-triggered fixed-time cooperative guidance law against maneuvering target with the constraint of relative impact angles, *J. Franklin Inst.*, **360** (2023), 3914–3966. https://doi.org/10.1016/j.jfranklin.2023.02.027
23. L. Ji, S. Tong, X. Guo, Y. Xie, H. Li, Anti-attack fuzzy tracking control for nonlinear multi-agent systems with topology switching, *Nonlinear Dyn.*, **113** (2025), 21403–21419. https://doi.org/10.1007/s11071-025-11219-8
24. H. Dai, L. Ji, X. Guo, C. Zhang, S. Yang, H. Li, Leader-following synchronization control of multiagent systems under hybrid cyber attacks via impulsive control based on topology switching, *IEEE Trans. Cybern.*, **54** (2024), 5297–5308. https://doi.org/10.1109/TCYB.2024.3367851
25. X. Liu, X. Chang, Adaptive event-triggered tracking control for nonlinear networked systems with dynamic quantization and deception attacks, *Int. J. Robust Nonlinear Control*, **34** (2024), 8311–8333. https://doi.org/10.1002/rnc.7389
26. S. Chen, W. Wang, J. Fan, Three-dimensional piecewise cooperative guidance with smooth switching topology, *Aerosp. Sci. Technol.*, **150** (2024), 109181. https://doi.org/10.1016/j.ast.2024.109181
27. H. Yu, K. Dai, H. Li, Y. Zou, X. Ma, S. Ma, et al., Three-dimensional adaptive fixed-time cooperative guidance law with impact time and angle constraints, *Aerosp. Sci. Technol.*, **123** (2022), 107450. https://doi.org/10.1016/j.ast.2022.107450
28. H. Yu, K. Dai, H. Li, Y. Zou, X. Ma, S. Ma, et al., Cooperative guidance law for multiple missiles simultaneous attacks with fixed-time convergence, *Int. J. Control*, **96** (2023), 2167–2180. https://doi.org/10.1080/00207179.2022.2086926
29. J. Ni, L. Liu, C. Liu, J. Liu, Fixed-time leader-following consensus for second-order multiagent systems with input delay, *IEEE Trans. Ind. Electron.*, **64** (2017), 8635–8646. https://doi.org/10.1109/TIE.2017.2701775

30. J. Zhao, H. Zhao, Y. Song, Z. Sun, D. Yu, Fast finite-time consensus protocol for high-order nonlinear multi-agent systems based on event-triggered communication scheme, *Appl. Math. Comput.*, **508** (2026), 129631. https://doi.org/10.1016/j.amc.2025.129631

31. J. Ni, L. Liu, Y. Tang, C. Liu, Predefined-time consensus tracking of second-order multiagent systems, *IEEE Trans. Syst. Man Cybern. Syst.*, **51** (2021), 2550–2560. https://doi.org/10.1109/TSMC.2019.2916257

32. B. Li, K. Qin, B. Xiao, Y. Yang, Finite-time extended state observer based fault tolerant output feedback control for attitude stabilization, *ISA Trans.*, **91** (2019), 11–20. https://doi.org/10.1016/j.isatra.2019.01.039

33. S. Zheng, H. Ma, H. Ren, H. Li, Practically fixed-time adaptive consensus control for multiagent systems with prescribed performance, *Sci. China Technol. Sci.*, **67** (2024), 3867–3876. https://doi.org/10.1007/s11431-024-2780-3

34. M. Panda, N. K. Peyada, A. Ghosh, Saturated adaptive backstepping control of uncertain nonlinear systems with validation using twin rotor system, *J. Franklin Inst.*, **357** (2020), 13477–13510. https://doi.org/10.1016/j.jfranklin.2020.10.003

35. Z. Wu, J. Guo, B. Liu, J. Ni, X. Bu, Composite learning adaptive dynamic surface control for uncertain nonlinear strict-feedback systems with fixed-time parameter estimation under sufficient excitation, *Int. J. Robust Nonlinear Control*, **31** (2021), 5865–5889. https://doi.org/10.1002/rnc.5582

36. Q. Zhou, W. Wang, H. Liang, M. V. Basin, B. Wang, Observer-based event-triggered fuzzy adaptive bipartite containment control of multiagent systems with input quantization, *IEEE Trans. Fuzzy Syst.*, **29** (2019), 372–384. https://doi.org/10.1109/TFUZZ.2019.2953573

37. X. Yu, Y. Lin, Adaptive backstepping quantized control for a class of nonlinear systems, *IEEE Trans. Autom. Control*, **62** (2016), 981–985. https://doi.org/10.1109/TAC.2016.2570140

38. J. Ni, Z. Wu, L. Liu, C. Liu, Fixed-time adaptive neural network control for nonstrict-feedback nonlinear systems with deadzone and output constraint, *ISA Trans.*, **97** (2020), 458–473. https://doi.org/10.1016/j.isatra.2019.07.013

39. S. Jiang, F. Tian, S. Sun, W. Liang, Integrated guidance and control of guided projectile with multiple constraints based on fuzzy adaptive and dynamic surface, *Def. Technol.*, **16** (2020), 1130–1141. https://doi.org/10.1016/j.dt.2019.12.003

40. Y. Liu, N. Xie, K. Li, Y. Liang, Missile guidance law design based on free-time convergent error dynamics, *J. Syst. Eng. Electron.*, **35** (2024), 1315–1325. https://doi.org/10.23919/JSEE.2024.000103

41. P. Surve, A. Maity, S. R. Kumar, Polynomial shaping based three-dimensional impact angle and field-of-view constrained guidance, *Aerosp. Sci. Technol.*, **147** (2024), 109018. https://doi.org/10.1016/j.ast.2024.109018

42. Z. Gao, J. Liu, J. Huang, W. Wang, W. Yi, S. Yuan, Three-dimensional fault-tolerant cooperative guidance law with constraints on relative impact velocity and attack angle, *Aerosp. Sci. Technol.*, **168** (2026), 111003. https://doi.org/10.1016/j.ast.2025.111003

43. Z. Gao, W. Yi, Integrated guidance and control design based on optimized sparrow search algorithm for sliding mode PID controller parameters, *Int. J. Aeronaut. Space Sci.*, **27** (2026), 791–810. https://doi.org/10.1007/s42405-025-00959-x

44. A. Levant, Higher-order sliding modes, differentiation and output-feedback control, *Int. J. Control*, **76** (2003), 924–941. https://doi.org/10.1080/0020717031000099029

45. A. Levant, Robust exact differentiation via sliding mode technique, *Automatica*, **34** (1998), 379–384. https://doi.org/10.1016/S0005-1098(97)00209-4

46. G. Li, Y. Wu, J. Liu, J. Zhao, Nonlinear transformed function-based adaptive finite-time integrated guidance and control design with full state constraints, *Aerosp. Sci. Technol.*, **143** (2023), 108723. https://doi.org/10.1016/j.ast.2023.108723

47. Z. Gao, W. Yi, J. Huang, J. Liu, Three-dimensional guidance law with precise control of attack time and constraints on attack angle, *ISA Trans.*, **167** (2025), 1228–1240. https://doi.org/10.1016/j.isatra.2025.09.028

48. X. Wang, H. Lu, X. Huang, Y. Yang, Z. Zuo, Three-dimensional time-varying sliding mode guidance law against maneuvering targets with terminal angle constraint, *Chin. J. Aeronaut.*, **35** (2022), 303–319. https://doi.org/10.1016/j.cja.2021.05.019

AIMS Press